Journal of the Australian Ceramic Society (2020) 56:233–241
https://doi.org/10.1007/s41779-019-00356-0

RESEARCH

The effects of graphene nanoplatelet addition to in situ compacted alumina nanocomposites using ultra-high frequency induction sintering system

İ. Murat Kuşoğlu[1] · Uğur Çavdar[2] · Ayberk Altintaş[3]

Received: 21 September 2017 / Revised: 3 April 2019 / Accepted: 5 May 2019 / Published online: 3 June 2019

Abstract

The aim of this study was to compact and sinter in situ graphene nanoplatelets (GNPs) with the addition of alumina (Al_2O_3) nanoparticles to form nanocomposites by using an ultra-high frequency induction sintering system with the assistance of applying a uniaxial load. To obtain the effect of the addition of GNPs to the compaction and to the mechanical properties of the nanocomposite, 1 to 5 wt.% GNPs was mixed to alumina nanoparticles by high-speed ball milling for 2 h at 350 rpm. Mixed Al_2O_3-GNP compositions were compacted in situ and sintered in a graphite die by induction-assisted heating at 1650 °C for 20 min with a uniaxial load applied in a vacuum chamber. The microstructure of as-sintered nanocomposites was observed using a scanning electron microscope (SEM) before and after thermal etching. Hardness and wear tests were carried out to determine mechanical properties. The results were compared with the properties of a pure alumina nanocompact. It was found that minimum grain size and maximum density, hardness, and wear resistance can be obtained by the addition of 1 wt.% GNPs to alumina nanoparticles. Higher amounts of GNP addition gradually decreased the density, hardness, and wear rates and increased the grain size of the alumina matrix.

Keywords Alumina · Graphene · Sintering · Induction · Nanocomposite

Introduction

Miniaturization in devices forces the powder metallurgy (PM) industry to use submicron and nanoparticles to produce micro-scale compact parts. As a general outcome, scientific studies proved that using nanoparticles to produce metal, ceramic, or composite-based PM materials improve physical and chemical properties [1–3]. Combining nanotechnology and powder metallurgy is a promising key field to obtain micro-scale multi-functional devices with superior properties [4–6]. PM techniques as in conventional sintering, hot isostatic pressing, ceramic injection molding, selective laser sintering, field-activated sintering, and spark plasma sintering are commonly used techniques to form complex shapes for engineering applications. On the other hand, using nanoparticles instead of micro-particles to produce micro-devices and micro-machines advances physical, chemical, and structural properties [7].

The particular case of compacting alumina-based nanocomposites has been widely studied. High wear and chemical resistance, high mechanical strength, and high electrical insulation of alumina maintain its characteristics in industrial applications. Producing a functional part from bulk or casted alumina by machining is not easy or cost effective due to its high hardness, elastic deformation property, low fracture toughness, and high melting point [8–12].

Using nanoparticles to form alumina-based nanocomposites, a rapid sintering cycle is needed. Furthermore, a secondary phase is required to avoid grain growth and higher sintering temperatures for better compaction and densification. These nanocomposites can be used for cutting tools, airplane industry, space industry, transparent conductors, and biosensors [13–15]. These novel composites are also often used in supercapacitors, lithium-ion batteries, transparent conductors, and biosensors [16].

✉ Uğur Çavdar
ugur.cavdar@idu.edu.tr

[1] Torbali Vocational School, Department of Industrial Glass & Ceramics, Dokuz Eylul University, Torbali Campus, Izmir, Turkey

[2] Engineering Faculty, Mechanical Engineering Department, İzmir Demokrasi University, İDU Campus, İzmir, Turkey

[3] Mechanical Engineering Department, Manisa Celal Bayar University, Muradiye Campus, 45400 Manisa, Turkey

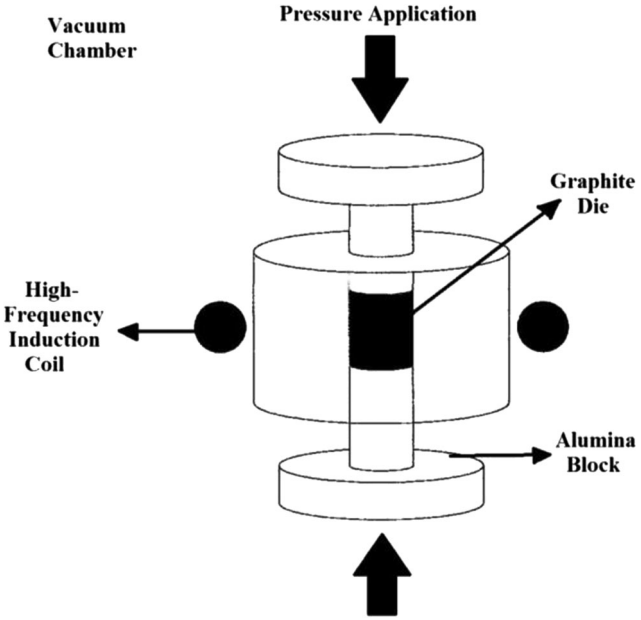

Fig. 1 Schematic diagram of the in situ compaction and sintering system [29]

Graphene additions to ceramic matrix composites develop thermal, electrical, wear, and mechanical properties [17–20]. Several studies claim that graphene-based nanosized reinforcements in an alumina matrix develop densification and avoid grain growth of the ceramic matrix [21, 22]. Graphene is a monolayer of hexagonal-oriented carbon atoms and has a two-dimensional morphology. Liu et al. [23] sintered alumina GNP nanocomposites by using spark plasma sintering (SPS) system and investigated the effects of GNP addition in the alumina matrix. Fan et al. [24] sintered alumina-few-layer graphene (FG) by the spark plasma sintering method and found that two-dimensional FG has a great ability to restrain grain growth in comparison to other inclusions. Nieto et al. [25] sintered GNP-Al_2O_3 nanocomposite by using SPS method for 3–10 min at 1100–1500 °C and found that over 5 vol.% GNP addition caused grain growth. Centeno et al. [26] sintered graphene oxide (GO)-alumina nanocomposites by using SPS method at 1300 °C and 1500 °C for 1 min. A trace amount of graphene addition was seen to improve the mechanical properties.

Table 1 Sintering parameters

Parameter	Applied value for induction sintering
Temperature	1650 °C
Power capacity	2.8 kW
Frequency	900 kHz
Duration	20 min
Cooling rate	Room temperature
Atmosphere	Vacuum (10^{-3} Torr)

Table 2 Sample codes given according to the composition of alumina nanoparticles and GNPs

Sample codes	Compositions (wt.%)	
	Al_2O_3	GNP
C0	100	0
C1	99	1
C2	98	2
C3	97	3
C4	96	4
C5	95	5

In this study, an alternative to spark plasma sintering was designed, combining a uniaxial load and an induction energy heating graphite die with rapid in situ compaction and sintering of nanoparticles. The most important feature of the induction system is rapid heating. Generally, it is used to heat-treated metals and metallic compacts [27]. Compared to the conventional heating systems, the advantages seen with heating with induction is the considerably shorter processing time; there is no environmental heat distribution, it is clean, highly productive, controllable, and repeatable. Furthermore, being subjected to a precise temperature control, no by-products are observed in the heating area and the system is secure without events, such as explosions happening [28]. While alumina does not interact with induction, a graphite die can be used to rapidly heat alumina nanoparticles up to sintering temperatures. To increase densification and to decrease sintering temperature and duration, the uniaxial load is adapted to the induction system. With this setup, alumina nanocomposites containing GNP with different ratios (1–5 wt.%) were in situ compacted and sintered by using an ultra-high frequency induction heating system in the graphite die under a vacuum at 1650 °C for 20 min. To determine

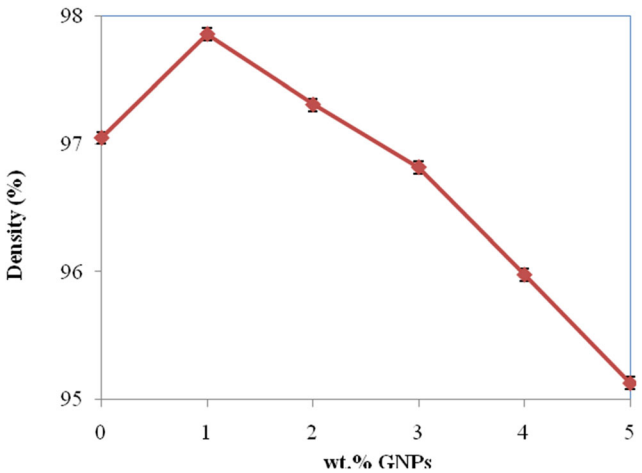

Fig. 2 The relative density of Al_2O_3-GNP nanocomposites (error range ± 0.055%)

Table 3 Surface roughness values (Ra, Ry, and Rz) for each sample (error range is ± 0.5 μm)

Code	Ra (μm)	Ry (μm)	Rz (μm)
C0	2.17	2.97	10.98
C1	1.51	4.44	6.12
C2	1.68	4.79	6.48
C3	1.94	5.02	6.77
C4	2.05	5.29	7.12
C5	2.11	5.99	7.74

the effect of GNP addition to alumina matrix, alumina nanoparticles are directly in situ compacted and sintered with the same sintering conditions. The effect of GNP addition was investigated throughout this work.

This work has been found to be useful for the PM industry which produces simple geometrical parts. It is particularly useful for manufacturers of structural parts for miniaturized devices.

Materials and methods

Alumina nanoparticles (44931 Alfa Aesar Aluminum Oxide NanoDur, the particle size of 40–50 nm, and purity of 99.5%) and graphene nanoplatelet aggregates (47132 Alfa Aesar, aggregates, sub-micron particles, S.A. 500 m^2/g) were used as raw materials. Alumina nanoparticles were mixed with various amounts of GNPs ranging between 1 and 5 wt.% by high-speed ball milling at 350 rpm for 2 h. The nanomixtures were placed in a graphite die (20 mm height; 10 mm inner diameter; 16 mm outer diameter) which was centered in the middle of the induction coil in a vacuum chamber. The schematic representation of the process is given in Fig. 1.

Sample codes are given in Table 2 according to amounts of alumina nanoparticles and GNPs. All nanomixtures were in situ compacted and sintered at 1650 °C for 20 min under a vacuum of 10^{-3} Torr by using 2.8 kW power and 900 kHz frequency induction system (Table 1). The temperature was measured using a laser infrared thermometer (± 5 °C) (Table 2).

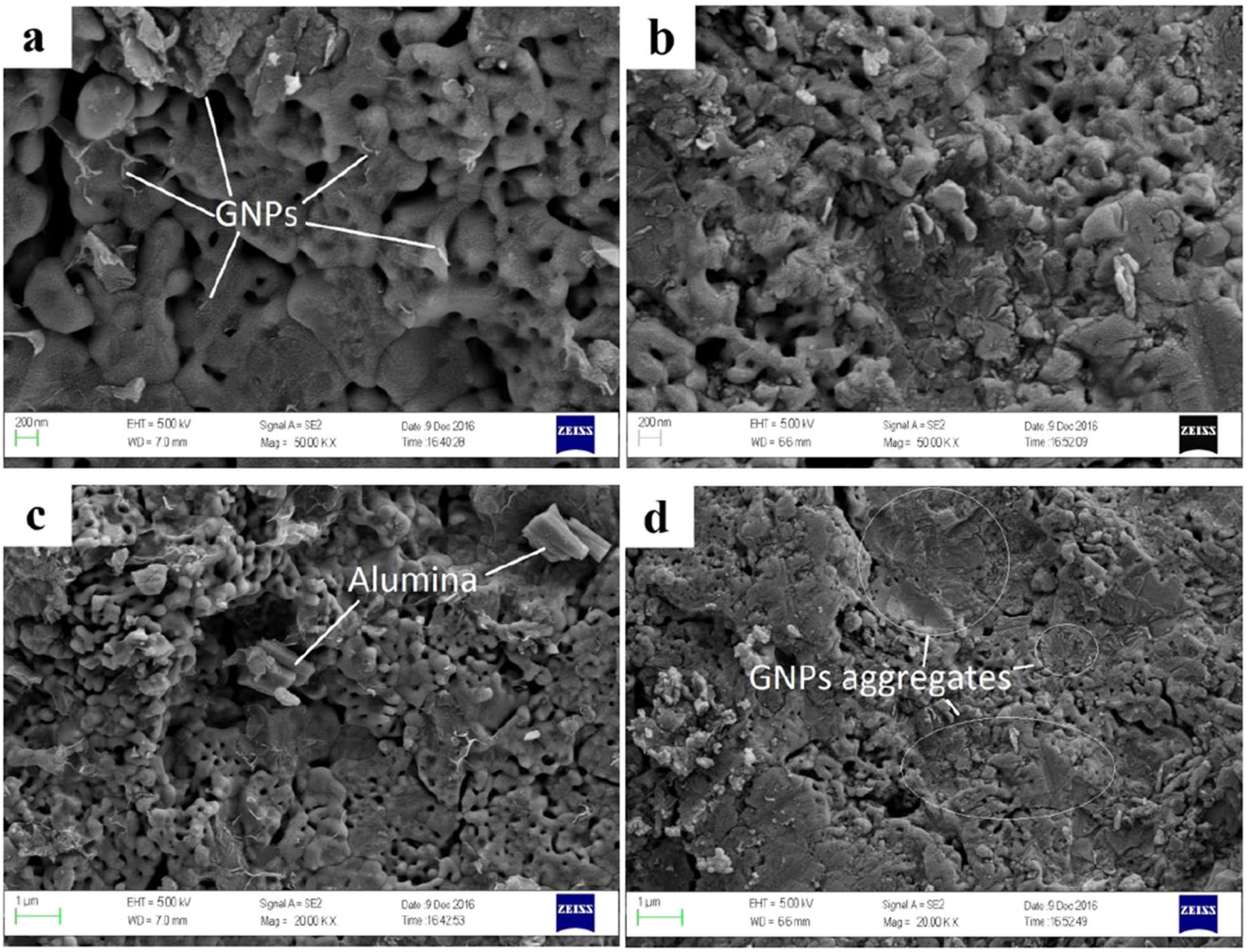

Fig. 3 SEM images of as-sintered **a** C1, **b** C5 at × 50000, and **c** C1, **d** C5 at × 20000 magnification

The relative densities of the as-sintered nanocomposites were measured by the Archimedes Method using the Radwag As 220/C/2 Archimedes Scale. The relative density was calculated from the bulk and theoretical density of as-sintered compacts according to their compositional ratios. The surface roughness tests were applied to as-sintered nanocomposites.

Microstructures of as-sintered nanocomposites were observed by a scanning electron microscope (SEM, Carl Zeiss

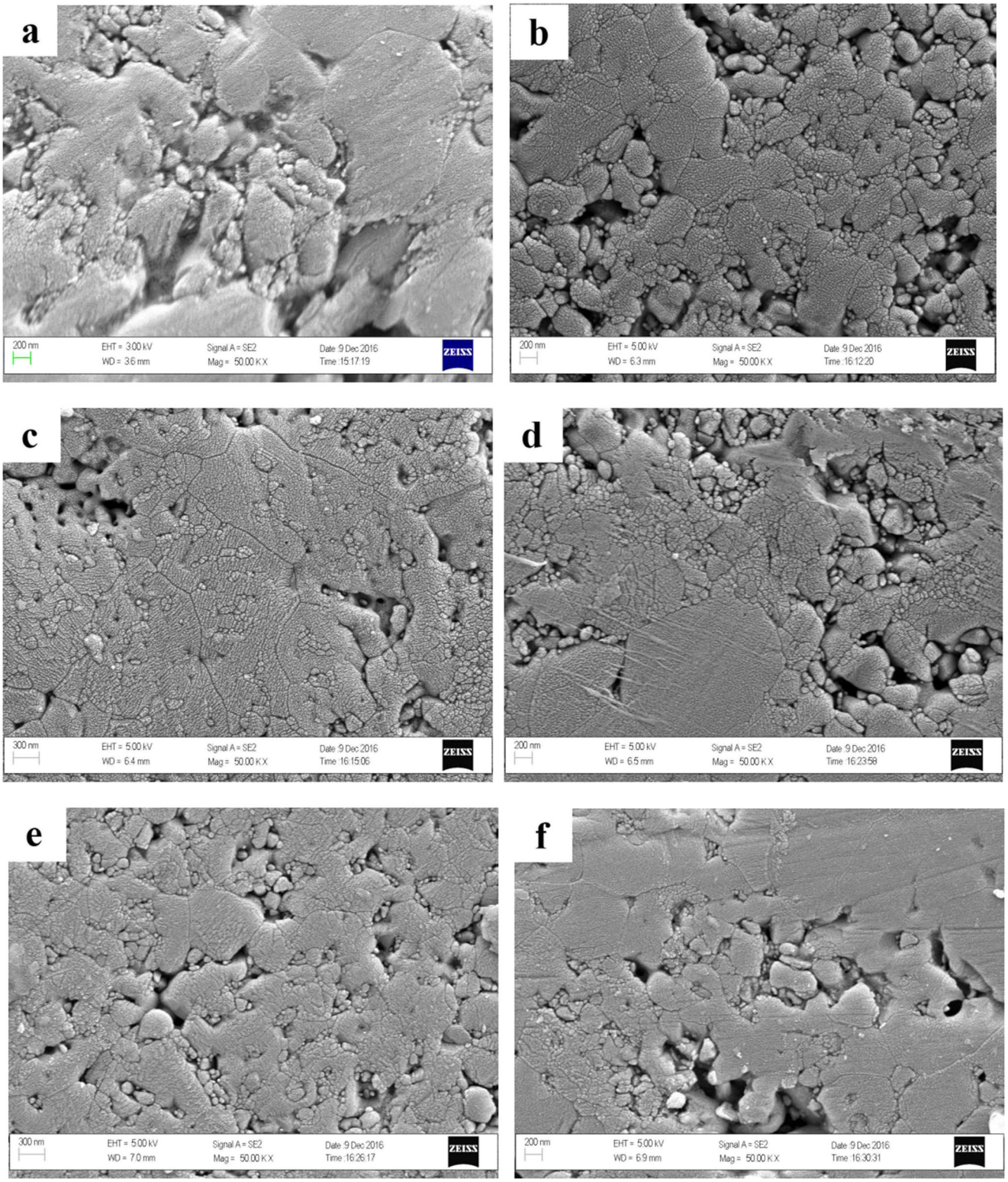

Fig. 4 Microstructures of thermally etched alumina-GNP nanocomposites of C0 (**a**), C1 (**b**), C2 (**c**), C3 (**d**), C4 (**e**), C5 (**f**) at × 50000 magnification

300VP) to obtain GNP distribution and the bonding structure of alumina grains. Additionally, as-sintered nanocomposites were polished by SiC grinding paper and thermally etched at 100 °C below the sintering temperature for 20 min to observe the grain size of the alumina matrix by SEM. X-ray diffraction (Thermo Fisher Scientific) was used to obtain phases of as-sintered compacts. The FM 700 Microhardness Tester machine was used for testing the hardness by applying 1 kg of force with 20-s dwell time. The average of five measurements was obtained for each sample. Surface roughness tests for Ra, Ry, and Rz values were carried out by the Mitutoyo Surf SJ-301 profilometer.

Wear experiments were carried out in the CMS Instruments Pin-on Disk Tribometer (0–60 N) using a circular motion. Before starting the test, each sample was ground with 1200 grade SiC paper to obtain the same surface roughness. A tungsten carbide (WC) ball was drawn over the surface for several revolutions in the same circular motion with a standard load of 10 N and a sliding speed of 10 cm/s. The test duration was associated with a traveling distance of 1000 m. The W which is the specific wear rate (mm^3/Nm) was calculated using Eq. (1) [25].

$$W = \frac{\Delta V}{F_N.S} \tag{1}$$

where ΔV is the volume loss after the test (mm^3), F_n is the applied load (N), and S is the sliding distance (m).

Results and discussion

Relative densities of as-sintered nanocomposites measured by the Archimedes' principle are shown in Fig. 2. It was found that pure alumina particles can be compacted to the relative density of 97%. It was found that 1 wt.% GNP addition developed a densification to 97.8%. This increase in density is most likely the result of good dispersion of GNPs in the matrix due to its 2D morphology and its lubricating effect that advanced the in situ compaction of alumina grains. When the amount of GNP addition increased, the relative density decreased gradually and was found to be 95.1% for 5 wt.% GNP addition. The gradual decrease of density in higher amounts of GNPs could be a sign of heterogeneous dispersion in the alumina matrix which will also cause agglomeration of GNPs in the matrix during high-speed ball-milling. The agglomeration of GNPs may have caused higher porosities between alumina-GNP grain boundaries and GNP aggregates; negatively affecting the packing of alumina grains in densification during sintering. On the other hand, deformation of GNP aggregates during in situ compaction opened an empty area between GNP layers that possibly increased the porosity level of nanocomposites.

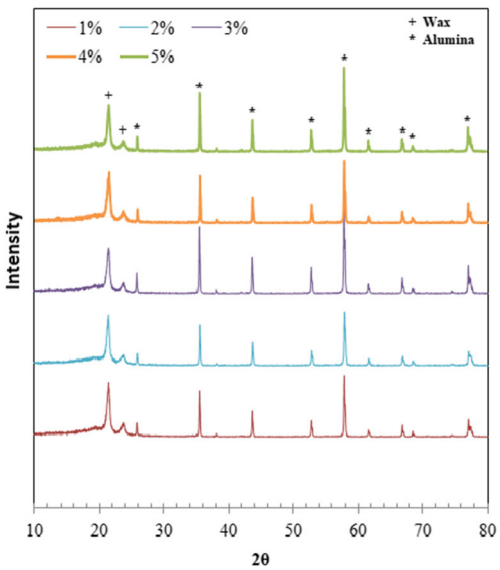

Fig. 5 XRD patterns of all nanocomposites

The surface roughness values of as-sintered nanocomposites were also measured. The values of Ra (arithmetical mean roughness), Ry (maximum peak), Rz (ten-point mean roughness) were obtained during the test. The arithmetic average of the three measurements from each compact is given in Table 3. The highest surface roughness values were observed for the pure alumina compact. The minimum surface roughness value was obtained for 1 wt.% GNP addition to alumina matrix. For GNP addition from 2 to 5 wt.% in the alumina matrix, the surface roughness of as-sintered nanocomposites gradually increased. Nampi et al. [30] studied the relation between surface roughness and grain size related to grain growth mechanism on the surface of alumina compacts and found that grain growth increases the surface roughness. Comparing the surface roughness results show that 1 wt.% GNP addition to the alumina matrix avoided grain growth and has possibly decreased the grain size. According to the surface roughness values, > 1 wt.% GNP addition gradually increased alumina grain sizes.

Microstructures of the as-sintered nanocomposite surfaces were observed by SEM. One weight percent and 5 wt.% GNP-added alumina nanocomposites are shown in Fig. 3. As seen in Fig. 3 a, alumina grains are rounded during grain growth and the porosities located at the grain boundaries are also rounded. Also, GNPs are homogeneously dispersed in the alumina matrix. Bended GNPs between alumina grains are indicated on the photo by white arrows. No GNP aggregates were observed in the microstructure, so GNP aggregates were successfully broken into small pieces and well distributed between the alumina nanoparticles during high-speed ball milling. As seen in Fig. 3 b, GNP aggregates can be observed clearly. This is a sign of insufficient or excess high-speed ball milling duration. The GNP aggregates are approximately 1–2 μm in size and cover the alumina grains like a blanket on the surface of the compact. Some coarse grains were also

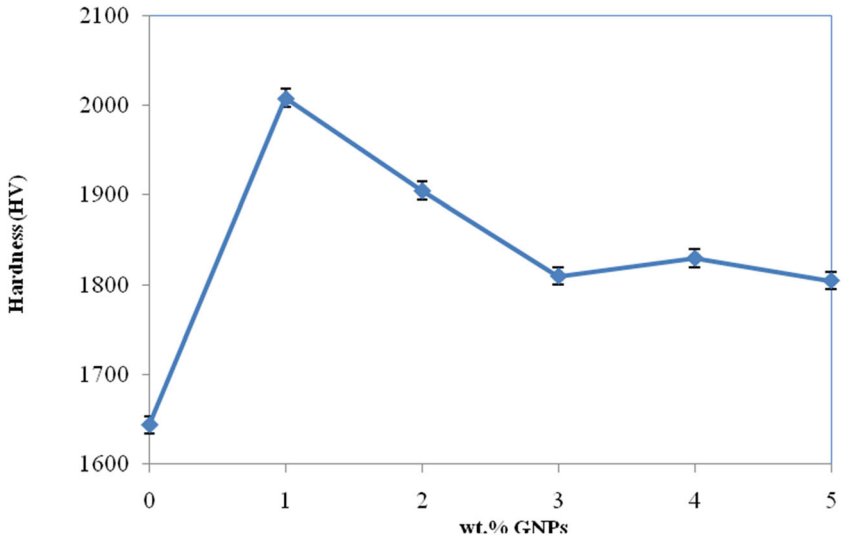

Fig. 6 Microhardness of sintered nanocomposites (error range ± 0.5%)

observed as seen in Fig. 3 a. A negligible amount of layered alumina grains were observed as in Fig. 3 c. Trace amount of coarse alumina grains formed during sintering can be seen in Fig. 3 c. The distribution of GNP aggregates can be seen in Fig. 3 d.

Thermal etching was applied to the as-sintered pure alumina nanocompact and alumina nanocomposites to observe the grain formation of alumina nanoparticles in the matrix during compacting and sintering. All compacts were thermally etched at 1550 °C for 20 min under air atmosphere. The thermally etched nanocomposites observed by SEM are given in Fig. 4. As a general outcome, GNP aggregates layered on the surface of the compact (Fig. 3) were burnt out by oxidation above 700 °C during the thermal etching process. Grain boundaries of the alumina grains consisting of alumina nanoparticles were clearly observed after thermal etching. When Fig. 4 a and b are compared, it is found that the addition of 1 wt.% GNPs distinctly decreased the grain size of the alumina matrix. The maximum grain size observed in C0 was 1.2 μm and decreased to 350 nm for C1. Homogeneous distribution of GNPs on the alumina grain boundaries caused pinning effects that decreased the alumina grain size [20]. Grain growth and coarser grains were gradually observed for higher amounts of GNP addition (Fig. 4b–d). As seen in Fig. 3 d, higher amounts of GNP aggregates in the matrix decreased the densification which provided more space for grain growth. Therefore, increasing the amount of GNPs in the alumina matrix increases the grain sizes of the alumina matrix. These observations support the surface roughness results given in Table 3. Higher surface roughness values can be related to grain growth of alumina.

XRD patterns of all the nanocomposites are given in Fig. 5. The crystalline intensity peaks around 21.5° and 23.5° are matched with the wax (JCPDS No.: 00-055-1330) used to

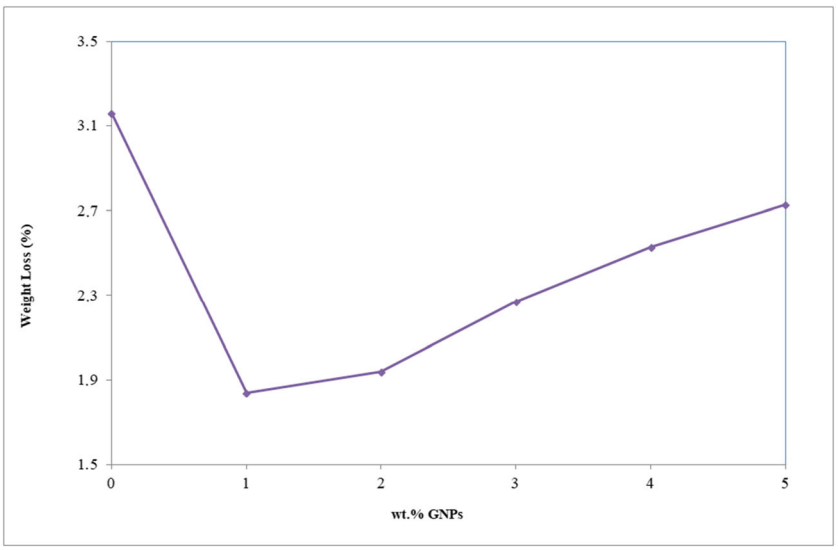

Fig. 7 Weight loss ratios of as-sintered compacts after ball-on-disc wear tests

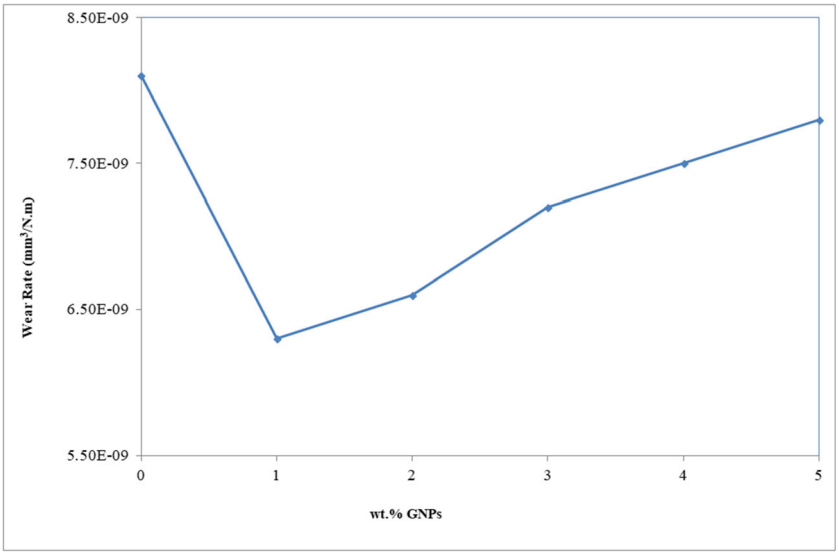

Fig. 8 Wear rates of as-sintered compacts after ball-on-disc wear tests

stabilize compacts during diffraction analyses. All alumina peaks obtained at nanocomposites were found to be in the corundum phase (JCPDS No.: 01-075-0784). I. Ahmad [29] obtained a crystalline graphite peak at 26.3° (JCPDS No.: 01-075-1621) and related that existence to the presence of graphene. However, no such graphitization is obtained in this study. W. Kim [31] also used up to 3 wt.% GNP addition to alumina, and again, did not obtain any crystalline graphite peak in XRD results.

The value of Vickers hardness was obtained from five different points of each compact and the arithmetic values are given in Fig. 6. The hardness value of pure alumina compact is around 1650 HV. While less residual porosity increases the hardness of ceramic compacts, a decrease in alumina grain size by GNPs located to grain boundaries also increases the hardness of C1. It is observed with the relative density results given in Fig. 2 that densification is improved by 1 wt.% GNP addition. Also, as seen in Fig. 4 a and b, the grain size of the alumina matrix is smaller for C1 compared to C0. As a result, the addition of 1 wt.% GNPs to alumina nanocomposite increases the hardness to 2000 HV which is nearly 20% higher than the pure alumina compact. > 1 wt. GNP addition decreases the hardness of nanocomposites due to a decrease in density and increase in grain size. The hardness value is found to be stabilized around 1820 HV > 3 wt.% GNP addition, which is still 12.5% higher than the pure alumina compact.

Wear lost (%) and wear rate (mm^3/Nm) results obtained after ball-on-disc wear tests are given in Fig. 7 and Fig. 8 respectively. The weight loss percent was obtained versus WC balls after 1000 m. Weight loss for the pure alumina compact was found to be 3.1%. One weight percent GNP addition decreased the weight loss percent to around 1.8, which means around a 42% decrease in weight loss. The decrease in grain size improved densification and adhesion of GNPs due to less surface friction and decreased weight loss % and wear rate. Greater than one weight percent GNP addition gradually increased the weight loss % and wear rate which was still below the results of the pure alumina compacts. GNPs have a lubricating effect during the wear test that develops wear properties [1]. Increasing the amount of GNP addition (> 1 wt.%) decreased the densification of nanocomposites and increased the grain size of alumina matrix that and adversely affected wear resistance. Minimum weight loss and minimum wear rate results were obtained for 1 wt.% GNP addition in the study. Increasing the amount of GNP addition adversely affected wear properties.

Conclusions

Pure Al_2O_3 nanoparticles and Al_2O_3-GNPs mixtures were successfully in situ compacted and sintered by UHFIHS system at 1650 °C for 20 min under a vacuum by applying a uniaxial load. All densification, hardness, grain size, and wear properties showed that 1 wt.% GNP addition has the optimum effect on compaction and mechanical properties among other GNP additions. One weight percent GNP addition to alumina nanoparticles decreased grain size, developed densification from 97 to 97.8%, increased hardness by 20%, decreased weight loss around 42%, and decreased the wear rate by 22.5%. Finer alumina grains are formed by GNP addition, improving the hardness and strength of the composites, due to the implication of dislocation movements caused by grain boundary pining effect. Greater than one weight percent GNP addition adversely affected densification and mechanical properties due to grain growth; even so, the results were better than the pure alumina compacts. In this study, it is found that the optimum addition of GNPs is 1 wt.%. Further studies can be focused on the addition of GNPs below 1 wt.% of alumina matrix and > 5 wt.% GNP addition to obtain a better

optimization. To increase the densification of nanocomposites, higher uniaxial loads can be applied which will possibly decrease the sintering temperature and/or duration. Also, longer high-speed ball milling may have better GNP distribution on the alumina grains. In addition, this technique can be applied to in situ compaction and sintering of ceramic nanoparticles.

Acknowledgments The research in this paper was supported by The Scientific and Technological Research Council of Turkey (Project Number: 214M414).

References

1. Gonzalez, C.F.G., Smirnov, A., Centeno, A., Fernandez, A., Alonso, B., Rocha, V.G., Torrecillas, R., Zurutuza, A., Bartolome, J.F.: Wear behavior of graphene/alumina composite. Ceram. Int. **41**, 7434–7438 (2015). https://doi.org/10.1016/j.ceramint.2015.02.061
2. Rodriguez-Suarez, T., Bartolomé, J.F., Smirnov, A., Lopez-Esteban, S., Dıaz, L.A., Torrecillas, R., Moya, J.S.: Electroconductive alumina–TiC–Ni nanocomposites obtained by spark plasma sintering. Ceram. Int. **37**(5), 1631–1636 (July 2011). https://doi.org/10.1016/j.ceramint.2011.01.033
3. Qin, Y., Zhao, J., Huang, K., Zulkipli, M., Hijji, H., Yang, Y., Wu, M., Yin, D.: Forming of miniature components from powders by combining field-activated sintering and micro-forming. Proc Eng. **207**, 1212–1217 (2017). https://doi.org/10.1016/j.proeng.2017.10.872
4. Drexler, K. Eric.: Engines of creation: the coming era of nanotechnology. Doubleday. ISBN 0-385-19973-2 (1986)
5. Drexler, K.E.: Nanosystems: molecular machinery, manufacturing, and computation. John Wiley & Sons**. ISBN 0-471-57547-X.**, New York (1992)
6. Mnyusiwalla, A., Daar, A.S., Singer, P.A.: 'Mind the gap': science and ethics in nanotechnology. Nanotechnology. **14**, (2013). https://doi.org/10.1088/0957-4484/14/3/201
7. J. Lawrence, A. Ostendorf, A. Neumeister, S. Dudziak, S. Passinger, J. Stampfl,: Chapter 20: micro- and nano-parts generated by laser-based solid freeform fabrication, Advances in Laser Materials Processing (Second Edition), 2018, Pages 595–633. https://doi.org/10.1016/B978-0-08-101252-9.00020-0
8. Yin, Z., Huang, C., Zou, B., Liu, H., Zhu, H., Wang, J.: Study of the mechanical properties, strengthening and toughening mechanisms of Al_2O_3/TiC micro-nano-composite ceramic tool material. Mater Sci Eng A. **577**, 9–15 (2013). https://doi.org/10.1016/j.msea.2013.04.033
9. Cheng, Y., Zhang, Y., Wan, T., Yin, Z., Wang, J.: Mechanical properties and toughening mechanisms of graphene platelets reinforced Al_2O_3/TiC composite ceramic tool materials by microwave sintering. Mater Sci Eng A. **680**, 190–196 (2017). https://doi.org/10.1016/j.msea.2016.10.100
10. Rahaman, M.N., Yao, A.Y., Bal, B.S., Garino, J.P., Ries, M.D.: Ceramics for prosthetic hip and knee joint replacement. J. Am. Ceram. Soc. **90**(7), 1965–1988 (2007). https://doi.org/10.1111/j.1551-2916.2007.01725.x
11. Borsa, C.E., Jones, N.M.R., Todd, R.I.: Influence of processing on the microstructural development and flexure strength of Al_2O_3/SiC nanocomposites. J. Eur. Ceram. Soc. **17**, 865–872 (1997). https://doi.org/10.1016/S0955-2219(96)00188-4
12. Chen, W.H., Lin, H.T., Nayak, P.K., Chang, M.P., Huang, J.L.: Sintering behavior and mechanical properties of WC-Al_2O_3 composites prepared by spark plasma sintering (SPS). Int. J. Refract. Met. Hard Mater. **48**, 414–417 (2015). https://doi.org/10.1016/j.ijrmhm.2014.10.016
13. Broniszewski, K., Wozniak, J., Czechowski, K., Jaworska, L., Olszyna, A.: Al_2O_3–V cutting tools for machining hardened stainless steel. Ceram. Int. **41**, 14190–14196 (2015). https://doi.org/10.1016/j.ceramint.2015.07.044
14. Broniszewski, K., Wozniak, J., Czechowski, K., Jaworski, L., Olszyna, A.: Al_2O_3–Mo cutting tools for machining hardened stainless steel. Wear. **303**, 87–91 (2013). https://doi.org/10.1016/j.wear.2013.03.002
15. Wozniak, Y.T., Trzaska, M., Cieslak, G., Cygan, T., Kostecki, M., Olszyna, A.: Preparation and mechanical properties of alumina composites reinforced with nickel-coated graphene. Ceram. Int. **42**, 8597–8603 (2016). https://doi.org/10.1016/j.ceramint.2016.02.089
16. Porwal, H., Tatarko, P., Grasso, S., Hu, C., Boccaccini, A.R., Dlouhý, I., Reece, M.J.: Toughened and machinable glass matrix composites reinforced with graphene and graphene-oxide nanoplatelets. Sci. Technol. Adv. Mater. 1–10 (2013). https://doi.org/10.1088/1468-6996/14/5/055007
17. Novoselov, K.S., Geim, A.K., Morozov, S.V., Jiang, D., Zhang, Y., Dubonos, S.V., Grigorieva, I.V., Firsov, A.A.: Electric field effect in atomically thin carbon films. Science. **306**(5696), 666–669 (2004). https://doi.org/10.1126/science.1102896
18. Lee, C., Wei, X., Kysar, J.W., Hone, J.: Measurement of the elastic properties and intrinsic strength of monolayer graphene. Science. **321**(5887), 385–388 (2008). https://doi.org/10.1126/science.1157996
19. Neto, A.H.C., Guinea, F., Peres, N.M.R., Novoselov, K.S., Geim, A.K.: The electronic properties of graphene. Rev. Mod. Phys. **81**(1), 109–162 (2009). https://doi.org/10.1103/RevModPhys.81.109
20. Chen, Y.F., Bi, J.Q., Yin, C.L., You, G.L.: Microstructure and fracture toughness of graphene nanosheets/alumina composites. Ceram. Int. **40**, 13883–13889 (2014). https://doi.org/10.1016/j.ceramint.2014.05.107
21. Channei, D., Nakaruk, A., Phanichphant, S.: Controlled oxidative aging time of graphite/graphite oxide to graphene oxide in aqueous media. J. Aust. Ceram. Soc. 1–6 (2017). https://doi.org/10.1007/s41779-017-0130-y
22. Gholami, F., Ismail, S., Noor, A.F.M.: Development of carboxylated multi-walled carbon nanotubes and bovine serum albumin reinforced hydroxyapatite for bone substitute applications. J. Aust. Ceram. Soc. **53**, 117 (2017). https://doi.org/10.1007/s41779-016-0016-4
23. Liu, J., Yan, H., Jiang, K.: Mechanical properties of graphene platelet-reinforced alumina ceramic composites. Ceram. Int. **39**, 6215–6221 (2013). https://doi.org/10.1016/j.ceramint.2013.01.041
24. Fan, Y., Estili, M., Igarashi, G., Jiang, W., Kawasaki, A.: The effect of homogeneously dispersed few-layer graphene on microstructure and mechanical properties of Al_2O_3 nanocomposites. J. Eur. Ceram. Soc. **34**, 443–451 (2014). https://doi.org/10.1016/j.jeurceramsoc.2013.08.035
25. Nieto, A., Huang, L., Han, Y.H., Schoenung, J.M.: Sintering behavior of spark plasma sintered alumina with graphene nanoplatelet reinforcement. Ceram. Int. **41**, 5926–5936 (2015). https://doi.org/10.1016/j.ceramint.2015.01.027
26. Centeno, A., Rocha, V.G., Alonso, B., Fernandez, A., Gutierrez-Gonzalez, C.F., Torrecillas, R., Zurutuza, A.: Graphene for tough and electrocontuctive alumina ceramics. J. Eur. Ceram. Soc. **33**, 3201–3210 (2013). https://doi.org/10.1016/j.jeurceramsoc.2013.07.007
27. Yoo, J.Y., Shon, I.J., Cho, B.H., Lee, K.T.: Fabrication and characterization of a Ni-YSZ anode support using high-frequency induction heated sintering (HFIHS). Ceram. Int. **37**, 2569–2574 (2011). https://doi.org/10.1016/j.ceramint.2011.04.002

28. Sevilay, Ç.: One phase induction heating system analysis and design. Master's Thesis, Pamukkale University, Institute of Science and Technology, Denizli/Turkey, (2005)
29. Ahmad, I., Islam, M., Abdo, H.S., Subhani, T., Khalil, K.A., Almajid, A.A., Yazdani, B., Zhu, Y.: Toughening mechanisms and mechanical properties of graphene nanosheet-reinforced alumina. Mater. Des. **88**, 1234–1243 (2015). https://doi.org/10.1016/j.matdes.2015.09.125
30. Nampi, P.P., Kume, S., Hotta, Y., Watari, K.: Effect of surface roughness on grain growth and sintering of alumina. Bull. Mater. Sci. **34**(4), 799–804 (July 2011). https://doi.org/10.1007/s12034-011-0197-y
31. Kim, W., Oh, H.-S., Shon, I.-J.: The effect of graphene reinforcement on the mechanical properties of Al2O3 ceramics rapidly sintered by high-frequency induction heating. Int. J. Refract. Met. Hard Mater. **48**, 376–381 (2015). https://doi.org/10.1016/j.ijrmhm.2014.10.011